RSC Advances

PAPER

View Article Online
View Journal | View Issue

Cite this: *RSC Adv.*, 2026, **16**, 4318

Comprehensive characterization and RSM-based optimization of crystal violet adsorption using $SnCl_2$–$FeCl_3$ and $SnCl_2$–$ZnCl_2$ activated pomegranate peel biosorbents

Nada Hamrouche,[ad] Chahrazed Djilani,[bc] Youghourta Belhocine,[ad] Nawal Bouzenad,[ad] Lehtihet Boudjema Amir,[g] Sabri Meradi,[a] Imene Hamrouche[ef] and Djihane Slimane Ben Ali *[ce]

This study investigates the potential of modified pomegranate peel biosorbents, specifically those activated with $SnCl_2$–$FeCl_3$ and $SnCl_2$–$ZnCl_2$, for the efficient removal of crystal violet (CV) dye from synthetic wastewater. The physicochemical properties of the prepared materials were examined using FTIR, SEM-EDX, XRD, TGA/DTG, BET, and pH_{pzc} analyses. Process optimization and modeling were performed using Response Surface Methodology (RSM) based on Central Composite Design (CCD), with statistical validation conducted through ANOVA. The modified pomegranate peel powders (PPP/Sn–Fe and PPP/Sn–Zn) exhibited enhanced adsorption efficiency, achieving maximum capacities of 675.47 mg g^{-1} and 357.18 mg g^{-1}, respectively. The adsorption behavior was best fitted by both the Langmuir and Freundlich isotherms, and followed a pseudo-second-order kinetic model. Thermodynamic evaluation confirmed that the process is spontaneous and endothermic. Additionally, the biosorbents demonstrated strong reusability, retaining high performance through up to seven adsorption/desorption cycles.

Received 1st December 2025
Accepted 30th December 2025

DOI: 10.1039/d5ra09290f

rsc.li/rsc-advances

1. Introduction

Over the centuries, continuous human and industrial expansion has placed growing stress on the natural environment, and the resulting impacts are now increasingly evident. Industries such as textiles and plastics are among the largest consumers of dyes and water, producing substantial quantities of colored wastewater that significantly deteriorate aquatic ecosystems.[1–3] Synthetic dyes, composed of complex organic molecules, are intentionally engineered to resist light exposure, chemical reactions, and microbial degradation, which makes them highly stable and persistent pollutants.[4] Crystal violet, a water-soluble cationic dye from the triphenylmethane group, is commonly used in the dyeing of materials like wool and nylon, as well as in ink and varnish production. However, CV is recognized for its toxic and carcinogenic effects, including skin irritation, kidney damage, and eye disorders.[5] Given these severe health and environmental risks, it is essential to develop advanced and sustainable treatment technologies to effectively remove such hazardous dyes from industrial effluents.[6]

Various methods such as biological degradation,[7] membrane filtration,[8] ion exchange,[9] electrochemical oxidation,[13] reverse osmosis,[12] and photo catalysis[13] have been explored for dye removal. Nevertheless, most of these techniques remain costly, energy-intensive, and often generate secondary pollutants. In contrast, adsorption stands out as an efficient and practical alternative for treating dye-laden wastewater, offering advantages such as operational simplicity, effectiveness at low dye concentrations, and ease of adsorbent regeneration.[14]

In recent years, numerous agricultural by-products have been investigated as low-cost biosorbents for CV removal, including coconut husk,[15] treated rice husk,[16] orange and banana peels,[17] moringa wastes,[18] and coffee waste.[19] Among these materials, pomegranate peel has attracted growing attention due to its strong ability to capture toxic pollutants from water. Commonly discarded as waste, this biomass is inexpensive, abundant, and rich in biopolymers such as

[a]Department of Process Engineering, Faculty of Technology, University of 20 Août1955, El Hadaiek Road, B. O. 26 21000 Skikda, Algeria. E-mail: n.hamrouche@univ-skikda.dz
[b]Faculté de Technologie, University of 20 Août1955, El Hadaiek Road, B. O. 26 21000 Skikda, Algeria
[c]Laboratory LRPCSI, University of 20 Août1955, El Hadaiek Road, B. O. 26 21000 Skikda, Algeria
[d]Laboratory of Catalysis, Bioprocess and Environment, Department of Process Engineering, Faculty of Technology, University of 20 August 1955, Skikda 21000, Algeria
[e]Department of Petrochemical, Faculty of Technology, University of 20 Août1955, El Hadaiek Road, B. O. 26 21000 Skikda, Algeria
[f]Laboratory of Chemical Engineering and Environment of Skikda, University of 20 August 1955 Skikda, Algeria
[g]Laboratory of Chemical Process Engineering, Department of Process Engineering, Faculty of Technology, Ferhat Abbas University Setif 1, Setif 19000, Algeria

cellulose, hemicellulose, lignin, and pectin. Its surface also contains oxygen-bearing functional groups; carboxyl, hydroxyl, and carbonyl that enhance dye adsorption. However, the efficiency of natural adsorbents often needs to be enhanced to reach performance levels compatible with industrial requirements.[20,21] Pomegranate peel, an abundant residue widely available in large quantities in Algeria, possesses porous structure rich in organic and inorganic compounds capable of binding them. It represents a viable alternative to conventional adsorbents in water treatment.[22,23] Physical and chemical activation methods are generally used to prepare activated carbon. The preparation process usually includes two phases (1) a carbonization phase, during which the raw material is pyrolyzed into a carbon precursor with fewer pores; (2) an activation phase, during which developed pores are generated by the action of an activator. Activation chemistries are relatively complex processes. Moreover, the use of corrosive and toxic activating chemicals such as KOH and H_3PO_4 for activation requires costly equipment and produces difficult to treat wastewater. New activation methods, such as template methods, are difficult to implement on an industrial scale due to their high cost. Consequently, the development of ecological and environmentally friendly adsorbent preparation methods is becoming increasingly important. In recent years, iron-based activators have been used to prepare activated carbon due to their low pollution, low corrosion, low cost, and the simplicity of their activation process. Studies show that $FeCl_2$ is similar to $FeCl_3$ and $ZnCl_2$, thereby facilitating the dehydration and aromatization of the biomass while preventing the formation of tar susceptible to clogging the pores.[24–26]

In this regard, the modification of biosorbents has been favored in recent years to modify the surface and thus improve their overall quality. Ultrasonication, which involves the application of ultrasonic waves, modifies the surface of the biomass through an acoustic cavitation mechanism. Few studies focus on the ultrasonic modification of adsorbents for pollutant treatment.[27] No study has yet focused on the biosorption of crystal violet using biosorbents modified by a mixture of $SnCl_2$/$FeCl_3$, $SnCl_2$/$ZnCl_2$, and ultrasonication.[10,11]

Response Surface Methodology (RSM) was employed in this study because it provides an efficient and statistically robust approach for optimizing adsorption processes. Unlike traditional one-factor-at-a-time methods, which cannot capture interactions between variables and require a large number of experiments, RSM enables the simultaneous evaluation of multiple parameters and their combined effects on system performance. This approach significantly reduces experimental effort while accurately identifying the optimal operating conditions.[28,29] Among the available RSM designs, the Central Composite Design (CCD) is particularly advantageous due to its flexibility, reliability, and successful application in numerous dye adsorption studies. Therefore, RSM–CCD was selected to ensure efficient optimization and a deeper understanding of the process variables.[30,31]

In this context, the objective of this study is to evaluate the performance of biosorbents modified using $SnCl_2$–$FeCl_3$ and $SnCl_2$–$ZnCl_2$ activating pairs for the removal of crystal violet (CV). Several experimental parameters influencing the adsorption process were investigated, including contact time, pH, temperature, initial dye concentration, and biosorbent mass. RSM based on the Central Composite Design (CCD) was employed to optimize various factors affecting the adsorption of CV dye. Suitable isotherm and kinetic models were applied to describe the adsorption process. The reusability of the developed biosorbents was thoroughly examined over multiple cycles. Overall, this study aims to enhance understanding of the activation and adsorption mechanisms and to propose optimized biosorbent formulations suitable for large-scale application in the sustainable treatment of dye-contaminated wastewater.

2. Materials and methods

2.1. PPP/Sn–Fe and PPP/Sn–Zn biosorbents preparation

The collected pomegranate peels were initially cut into small fragments to facilitate washing, drying, and grinding. They were thoroughly rinsed with distilled water to remove impurities and subsequently dried in a Digit Heat TFT oven (JP Selecta, Barcelona, Spain) at 105 °C with a heating rate of 5 °C min^{-1} for 20 h. The dried material was then ground using a SILVERCREST 500G Electric Grinder (Europe, Germany) and sieved to obtain a uniform particle size. The resulting powder was divided into two batches for chemical activation.

For the first modification, 5 g of the raw pomegranate peel powder (PPP) was combined with a solution containing 1 g of $SnCl_2 \cdot 2H_2O$ (10 025-69-1) and 1 g of $FeCl_3 \cdot 6H_2O$ (10 025-77-1), producing the PPP/Sn–Fe biosorbent. Similarly, another 5 g portion of PPP was treated with a solution prepared from 1 g of $SnCl_2 \cdot 2H_2O$ (10 025-69-1) and 1 g of $ZnCl_2$ (7646-85-7) in a 100 mL volumetric flask, yielding PPP/Sn–Zn biosorbent. Each suspension was sonicated for 3 h at room temperature using an Elmasonic 100 7137 S10H ultrasonic bath (Germany) to ensure homogeneous mixing. After sonication, the mixtures were oven-dried at 60 °C for 24 h, then immersed in HCl (7647-01-0) 0.1 M for 30 min under continuous stirring to remove residual activating agents. The materials were subsequently washed with distilled water until the filtrate reached pH ≈ 7, as verified by a Lab pH meter inoLab pH 7110 (WTW, Germany). Finally, the samples were dried again at 105 °C (5 °C min^{-1}) for 24 h, finely ground, and sieved to achieve a final particle size of 150–250 μm.

2.2. PPP/Sn–Fe and PPP/Sn–Zn characterization

The surface properties of the modified biosorbents, PPP/Sn–Fe and PPP/Sn–Zn, were examined using several advanced characterization techniques. Fourier Transform Infrared Spectroscopy (FTIR-ATR, Bruker) was used to identify the functional groups present on the biosorbents surfaces before and after the adsorption process. The crystalline structure of the materials was analyzed by X-ray diffraction (XRD) at ambient temperature using a PANalytical Empyrean diffractometer. Thermal stability was evaluated through thermogravimetric analysis (TGA). The morphology and surface elemental composition of the adsorbents were investigated using a scanning electron microscope

(SEM/FEG: Quattro S) equipped with an energy-dispersive X-ray (EDX) detector. The textural characteristics including specific surface area, pore volume, and pore size distribution were determined using Brunauer–Emmett–Teller (BET), Barrett–Joyner–Halenda (BJH), and Dollimore–Heal (DH) methods on a Quantachrome Autosorb iQ3 high-vacuum physisorption/chemisorption analyzer. Prior to these analyses, the samples were degassed at 200 °C for 8 h to remove any physically adsorbed species. Subsequent nitrogen adsorption–desorption measurements were performed at −196 °C (77 K).

The point of zero charge (pH_{pzc}) of the biosorbents was also determined to understand the influence of pH on surface charge behavior, an important factor in adsorption governed by electrostatic interactions.[32] For this purpose, 0.15 g of each adsorbent was added to 50 mL of NaCl solution (7647-14-5) 0.01 M in 100 mL flasks. The initial pH of each suspension was adjusted between 1 and 10 using HCl (7647-01-0) or NaOH (1310-73-2) 1 M, and the mixtures were stirred magnetically at 250 rpm for 24 h at room temperature.[33] The pH_{pzc} corresponds to the point at which the final pH equals the initial pH, indicating that the surface carries no net electrical charge.[34]

2.3. Adsorption study in batch mode

Adsorption studies were performed at room temperature using a set of Erlenmeyer flasks, each containing a specific amount of adsorbent mixed with 50 mL of a crystal violet dye solution (548-62-9) at a known concentration. The influence of several key operational factors on the adsorption performance was systematically investigated, including contact time (5, 10, 20, 30, 40, 50, 60, 90, 120 and 180 min), adsorbent dosage (0.025, 0.05, 0.1, 0.15 and 0.2 g), initial dye concentration (5, 10, 20, 50 and 100 mg L^{-1}), solution pH (2, 4, 6, 8 and 10), and temperature (20, 30, 40, 50 and 60 °C). The dye removal efficiency (R, %) from the aqueous phase was calculated using the following relation:

$$\%R = \frac{(C_0 - C_e)}{C_0} \times 100 \quad (1)$$

In this equation, C_0 and C_e (mg L^{-1}) denote the initial and equilibrium concentrations of CV dye, respectively. A fixed amount of adsorbent was introduced into the dye solutions, and the mixtures were stirred at 250 rpm using a magnetic stirring system until adsorption equilibrium was achieved. The adsorbent–dye suspensions were then separated *via* centrifugation using a high-speed refrigerated centrifuge (DragonLab D3024R, China). The supernatants were filtered, and the residual dye concentration was measured using a UV-vis spectrophotometer (SHIMADZU UV-1900i, Japan) at a wavelength of 590 nm. The adsorption capacities at equilibrium (q_e, mg g^{-1}) and at a given time (q_t, mg g^{-1}) were calculated using the following equations. Where V is the solution volume (L), m is the adsorbent mass (g), and C_t (mg L^{-1}) the dye concentration at time t.

$$q_e = \frac{C_0 - C_e}{m} \times V \quad (2)$$

$$q_t = \frac{C_0 - C_t}{m} \times V \quad (3)$$

2.4. Kinetic and equilibrium analysis of the adsorption process

Adsorption kinetics provide essential insights into the rate and mechanism of pollutant uptake, helping to identify the controlling steps of the process.[29] To interpret the experimental data, pseudo-first-order (PFO), pseudo-second-order (PSO) and Intraparticle diffusion kinetic models, along with the Langmuir, Freundlich and Temkin isotherm models, were applied using their respective non-linear equations summarized in Table S1.[35] These models were used to describe the adsorption behavior of CV onto PPP/Sn–Fe and PPP/Sn–Zn modified biosorbents.

2.5. Optimization of adsorption parameters using RSM

Response surface methodology is a statistical optimization technique widely applied to enhance the performance of modified biomass adsorbents in removing organic pollutants.[36] Among its experimental designs, the CCD model is the most frequently employed for modeling and process optimization with fewer experimental runs.[37] In this study, RSM was used to evaluate the influence of four key variables; initial dye concentration (A), pH (B), temperature (C), and adsorbent dosage (D) on adsorption capacity. The parameter ranges are summarized in Table 1. The CCD model was applied to identify optimal conditions for efficient dye removal using a quadratic second-order model, as represented in eqn (4).

$$Y = \beta_0 + \sum_{(i=0)}^{n} \beta_i X_i + \sum_{(i=0)}^{n} \beta_{ii} X_i^2 + \sum_{(i=1)}^{(n-1)} \sum_{(j=1+1)}^{n} \beta_{ij} X_i X_j \quad (4)$$

In this model, Y represents the predicted response, and X denotes the independent variables. The coefficients β_0, β_j, β_{jj}, and β_{ij} correspond to the intercept, linear, quadratic, and interaction effects, respectively, while n indicates the number of coded variables. The adequacy of the quadratic model was assessed using the coefficient of determination (R^2) and Fisher's F-test. Model fitting, accuracy, and statistical significance were evaluated through analysis of variance (ANOVA) using Design-Expert 13 software. At a 95% confidence level, models

Table 1 CCD experimental range and levels of input process variables assessed

Variables	Symbol	Low (−1)	Central (0)	High (1)
Initial concentration (mg L^{-1})	A	5	52.5	100
Initial pH	B	2	6	10
Temperature (°C)	C	20	40	60
Adsorbent dosage (g)	D	0.025	0.1125	0.2

exhibiting higher *F*-values and lower *p*-values were considered statistically significant, indicating a strong correlation between the experimental and predicted results.[38]

During the adsorption experiments of CV dye, the Central Composite Design was applied within the Response Surface Methodology framework to examine the influence of key process variables on the biosorption capacity (q_e, mg g^{-1}). Four operational factors were evaluated using a full face-centered CCD comprising 29 experimental runs (Tables S2 and S3). In this model, N represents the number of experimental runs, k the number of independent variables, and C the number of central points, as defined in eqn (5). The design included 16 factorial points, 8 axial points, and 1 central point, with an additional 4 replicates at the center to accurately estimate experimental error. The sequence of runs was determined according to the experimental design plan. To explore both individual and interactive effects of the variables, a total of 29 experiments was conducted for CCD model.[31]

$$N = 2^k + 2k + C = 2^4 + 2 \times 4 + 5 = 29 \quad (5)$$

2.6. Regeneration studies

The assessment of the activity, stability, and reusability of the prepared biosorbents represents an essential step in evaluating their practical applicability. In adsorption systems, regeneration is the most common approach for restoring adsorbent performance and ensuring multiple reuse cycles. This process involved desorbing the adsorbate (CV dye) from the biosorbent materials (PPP/Sn–Fe and PPP/Sn–Zn) to restore their adsorption capacity for reuse. Following the completion of the adsorption process, the regenerated biosorbent materials were recovered from the desorbing solution through filtration. Subsequently, they underwent repeated washing using distilled water to remove any residual traces of the desorbing medium or adsorbate. No chemical regenerant was used; this simple washing provided an eco-friendly way to remove CV molecules without affecting the biosorbent's structure or surface chemistry. Finally, the regenerated biosorbents were dried up in an oven at 80 °C to remove residual moisture, rendering them ready for reuse in subsequent adsorption cycles. The adsorbents were fully loaded under the initial adsorption conditions before each regeneration cycle, using the optimal parameters (initial CV dye concentration, dose, pH, temperature, and contact time) to ensure maximum dye uptake. Through this regeneration process, the biosorbent materials can be effectively reused multiple times, enhancing the overall efficiency and sustainability of the adsorption process.[39,40] The adsorption capacities were calculated using eqn (2), where the parameters C_0 and C_e are defined in Section 2.4.

2.7. Assessment of microbial toxicity

The microbial toxicity of CV dye before and after adsorption was evaluated using three reference bacterial strains obtained from the Algerian Pasteur Institute: *Staphylococcus aureus* ATCC® 6538 (Gram-positive), *Pseudomonas aeruginosa* ATCC® 27 853, and *Escherichia coli* ATCC® 25 922 (both Gram-negative). The antibacterial activity of the dye and its degradation products was assessed through an agar diffusion assay. Each strain was cultivated in nutrient broth at 37 °C for 18 h, and the bacterial inoculum was adjusted to an optical density of 0.08–0.1 at 620 nm. The suspensions were then spread uniformly over Muller–Hinton agar plates. Sterile discs were impregnated with 30 µL of 100 mg L^{-1} CV solutions (before and after adsorption onto PPP/Sn–Fe and RPP/Sn–Zn) and placed on the agar surface. The plates were incubated at 37 °C for 24 h, after which inhibition zones were measured to determine the extent of microbial toxicity.

3. Results and discussion

3.1. Analytical techniques and characterization

The functional active groups present in the PPP/Sn–Fe and PPP/Sn–Zn structures, both before and after adsorption, were identified through FTIR analysis. The FTIR results are presented in

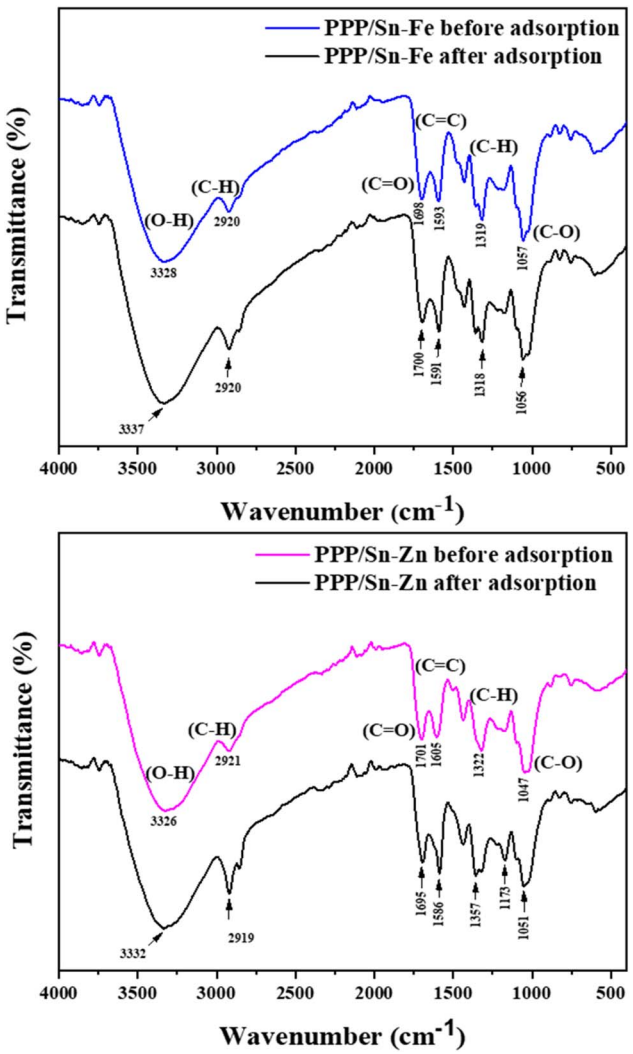

Fig. 1 FTIR spectra of PPP/Sn–Fe, PPP/Sn–Zn before and after adsorption.

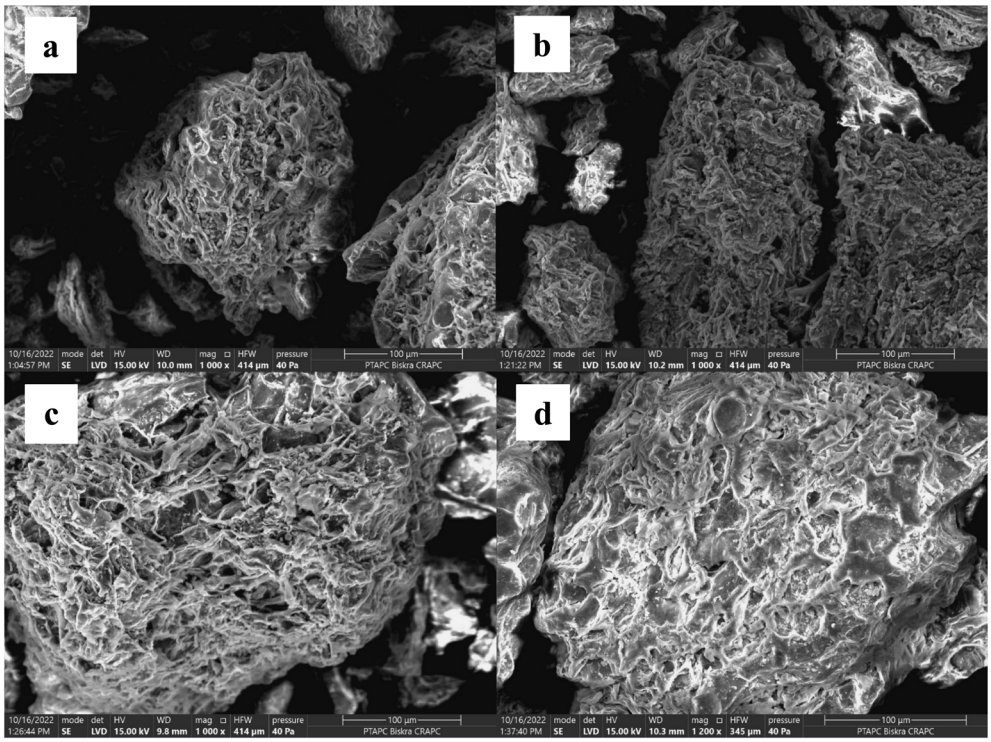

Fig. 2 SEM image of (a), PPP/Sn–Fe; (b) PPP/Sn–Fe -CV; (c) PPP/Sn–Zn; and (d) PPP/Sn–Zn -CV.

Fig. 1. After the biosorbents were modified, it was observed that the majority of bands in the adsorbents structure remained at the same position, indicating that the intrinsic structure of the natural adsorbent was preserved an important factor in maintaining its adsorption performance. This preservation is crucial as it ensures that the fundamental structural integrity of the adsorbent is maintained, which is essential for its effectiveness in adsorption processes.[41] A noticeable increase in the intensity of certain IR bands suggested partial bond cleavage during the activation process when comparing the spectrum of both PPP/Sn–Fe and PPP/Sn–Zn to previously studied biosorbents, particularly natural materials such as unmodified pomegranate peel.[42]

In Fig. 1, the peaks at 3328 and 3326 cm^{-1} for PPP/Sn–Fe biosorbent and at 1057 and 1047 cm^{-1} for PPP/Sn–Zn biosorbent, are the spectral features in the natural pomegranate peel. The absorption bands around 3328 and 3326 cm^{-1} corresponds to the stretching mode of – OH groups while the highly intense peak at 1057 and 1047 cm^{-1} are assigned to –C–O– linkage in phenolic, alcoholic, and carboxyl groups.[23,43] The observed peaks at 2920 and 2921 cm^{-1} are attributed to the C–H stretching vibrations.[44] The peaks located at 1698 cm^{-1}, 1701 cm^{-1} and 1593 cm^{-1}, 1605 cm^{-1} could be assigned to the stretching of C=O and the vibration of C=C bonds from the aromatic rings, respectively, indicating that raw peels contain hydroxyl and carbonyl groups, as well as polyphenol groups.[45] After CV dye adsorption onto the PPP/Sn–Fe and PPP/Sn–Zn surfaces, the FTIR spectra exhibited similarities between biosorbents both before and after adsorption, the transmittance of the peaks for dye-loaded biosorbents either shifted or slightly decreased after adsorption, as shown in Fig. 1. The slight variation in wavenumbers between the biosorbents before and after adsorption reflects the adsorptive interaction between the CV dye molecules and the PPP/Sn–Fe and PPP/Sn–Zn surfaces. This suggests the involvement of the main functional groups of both biosorbents in CV dye adsorption.[46,47]

The surface morphology and porous structure of PPP/Sn–Fe and PPP/Sn–Zn biosorbents were characterized using SEM–EDX analysis. In Fig. 2, SEM micrographs illustrate the surface features of PPP/Sn–Fe (a, before; b, after adsorption of CV) and

Table 2 Elemental composition of biosorbents, the values of surface area and pore volume obtained through BET

	Atomic (%)						Textural parameters		
Biosorbents	C	O	Cl	Fe	Sn	Zn	Surface area ($m^2\ g^{-1}$)	Pore volume ($cm^3\ g^{-1}$)	Pore size (nm)
PPP/Sn–Fe	40.7	54.4	0.16	0.52	4.15	—	17.7	0.48	54.6
PPP/Sn–Zn	46.03	50.9	0.60	—	1.78	0.62	13.9	0.35	50.9

PPP/Sn–Zn (c, before; d, after adsorption of CV). Fig. 2a and c depicted that both biosorbents exhibited a rough and highly porous surface, differing markedly from the unmodified pomegranate peel surface,[42] This pronounced surface roughness and pore development are indicative of successful chemical activation and are expected to enhance adsorption performance by increasing the available surface area and the number of accessible active sites.[22] The EDX test further validated the successful modification by detecting characteristic elements such as Sn, Fe, Cl, and Zn on the biosorbents surface with the main constituents in the PPP (carbon and oxygen) as listed in Table 2. The morphological characteristics of both PPP/Sn–Fe and PPP/Sn–Zn were altered after the adsorption of the CV dye (Fig. 2b and d), resulting in a decrease in porosity and cracks, which is consistent with the amount of dye loaded onto the biosorbents surface,[47] indicating a successful adsorption of CV dye molecules onto the surfaces of PPP/Sn–Fe and PPP/Sn–Zn biosorbents.

The crystalline or amorphous structure of PPP/Sn–Fe and PPP/Sn–Zn biosorbents were examined using XRD analysis. As shown in Fig. 3. The diffraction patterns exhibited new peaks at 26.8° and 26.6° PPP/Sn–Fe and at 22.7° and 22.1° for PPP/Sn–Zn, with a notable change in intensity attributed to the use of the activating agents ($SnCl_2$–$FeCl_3$ and $SnCl_2$–$ZnCl_2$) in comparison with the raw pomegranate peel studied previously.[42] The XRD plot analysis of both samples also revealed the absence of prominent sharp peaks that could be assigned to the crystal line structure.[23] The amorphous nature of the biosorbents promotes enhanced diffusion of CV dye molecules toward the surface and internal regions of the material.[48,49] This structural characteristic of the biosorbents is mainly attributed to the high content of lignin, cellulose, and hemicellulose, which disrupt crystalline order and contribute functional groups favorable for adsorption.[50]

Fig. 4 presents the thermogravimetric (TGA) and differential thermal (DTA) curves of PPP/Sn–Fe and PPP/Sn–Zn biosorbents.

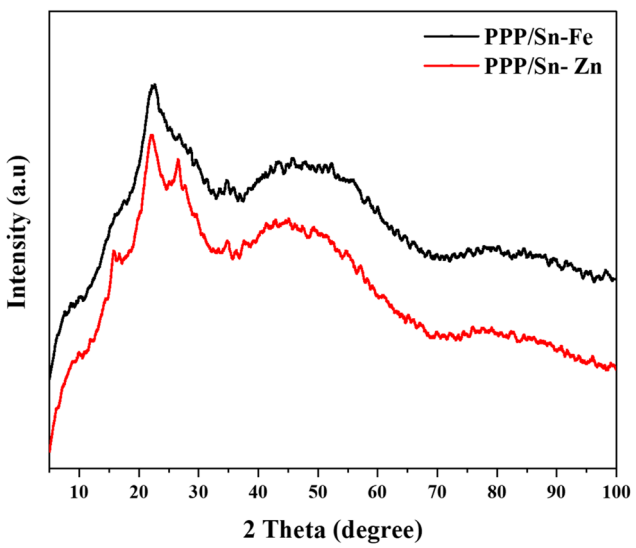

Fig. 3 X-ray diffraction patterns of PPP/Sn–Fe and PPP/Sn–Zn.

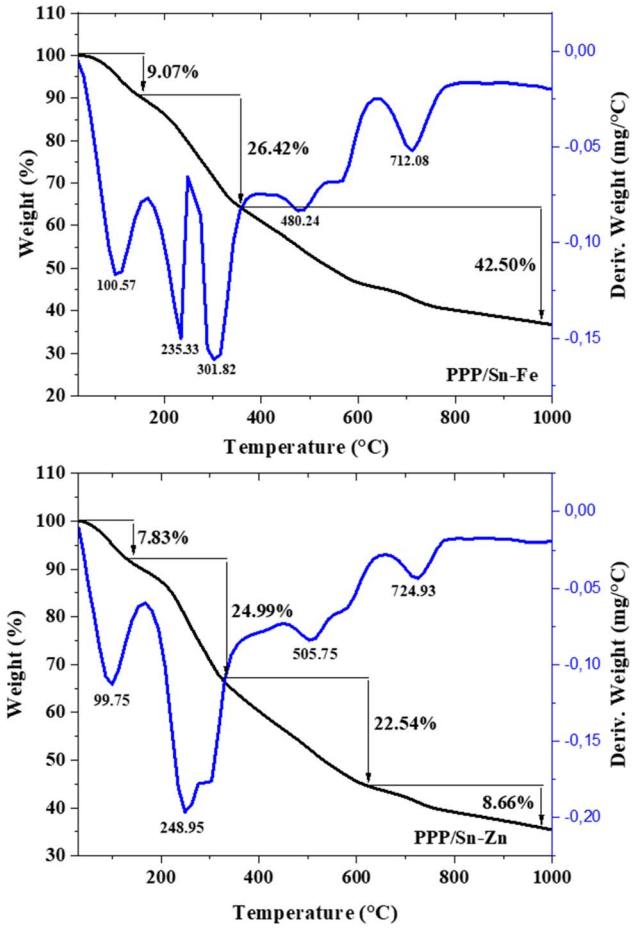

Fig. 4 TGA/DTG analysis of PPP/Sn–Fe and PPP/Sn–Zn.

Both materials display a typical three-stage thermal decomposition behavior of lignocellulosic materials up to 1000 °C. The initial mass loss below 165 °C is attributed to the evaporation of physically adsorbed moisture. The second stage corresponds to the decomposition of surface functional groups such as hydroxyl and carboxyl,[42] while the final stage is associated with the thermal degradation of the organic matrix. The DTA profiles reveal two main endothermic peaks: the first (140–300 °C) related to hemicellulose degradation and the second (300–400 °C) attributed to cellulose decomposition.[45,51]

The nitrogen adsorption–desorption isotherms of PPP/Sn–Fe and PPP/Sn–Zn adsorbents are presented in Fig. 5, while the corresponding textural parameters are summarized in Table 2. According to the IUPAC and BDDT (Brunauer–Deming–Deming–Teller) classifications,[52,53] both materials display type III isotherms with H3-type hysteresis loops, characteristic of solids composed of aggregated plate-like particles that generate slit-shaped pores.[54] The hysteresis behavior also reflects the influence of pore-network connectivity. BET analysis showed that PPP/Sn–Fe and PPP/Sn–Zn possess specific surface areas of 17.7 $m^2\ g^{-1}$ and 13.9 $m^2\ g^{-1}$, and total pore volumes of 0.483 $cm^3\ g^{-1}$ and 0.356 $cm^3\ g^{-1}$, respectively, demonstrating a substantial increase compared with the unmodified PP.[42] As shown in Table 2, the pore size distribution confirmed the macroporous nature of both materials (54.6 nm and 50.9 nm).

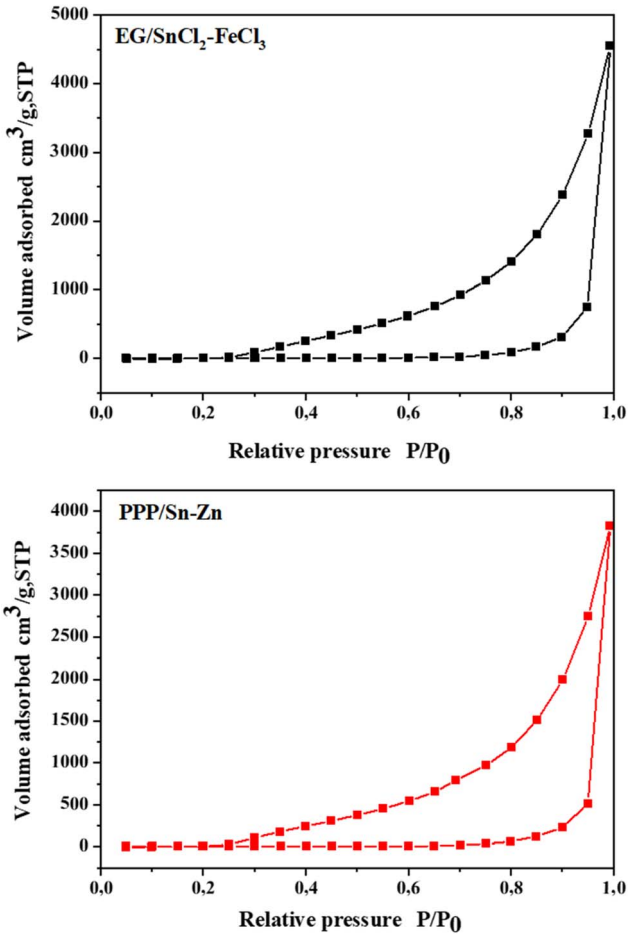

Fig. 5 N_2 adsorption–desorption isotherm of PPP/Sn–Fe and PPP/Sn–Zn biosorbents.

These results indicate that chemical activation using $SnCl_2$–$FeCl_3$ and $SnCl_2$–$ZnCl_2$ effectively improves the structural and surface properties of the biosorbents by enlarging their specific surface area and pore volume.

3.2. The point of zero charge pH_{pzc}

The influence of solution pH on the adsorption of CV onto PPP/Sn–Fe and PPP/Sn–Zn was interpreted based on their points of zero charge (pH_{pzc}). The pH_{pzc} values were found to be approximately 3.83 for PPP/Sn–Fe and 5.41 for PPP/Sn–Zn. When the pH of the solution exceeds the pH_{pzc}, the adsorbent surface becomes negatively charged due to the deprotonation of basic functional groups, promoting electrostatic attraction with the cationic CV molecules. In contrast, at pH values below the pH_{pzc}, protonation of acidic groups leads to a positively charged surface, which hinders cation adsorption and favors anionic species.[50,55] Therefore, the pH_{pzc} provides valuable insight into the surface charge behavior of the modified adsorbents under different pH conditions, directly influencing their adsorption performance toward CV dye.

3.3. Adsorption performance

3.3.1. Effect of initial dye concentration and contact time. As depicted in Fig. S1, the adsorption behavior of CV at varying initial concentrations (5–100 mg L^{-1}) was monitored over contact times ranging from 0 to 180 min for both adsorbents. The removal efficiency increased steadily with time and reached equilibrium after approximately 90 min for PPP/Sn–Fe and PPP/Sn–Zn. At lower concentrations, CV molecules readily occupy the available active sites on the adsorbent surfaces. However, as the dye concentration increases, these sites become progressively saturated, leading to a decline in removal efficiency.[56] The adsorption process proceeds in three distinct phases: an initial rapid uptake within the first 10 min due to the abundance of vacant sites, a slower diffusion-controlled phase (20–40 min) as active sites become limited, and finally, a plateau phase around 90 min, corresponding to near-saturation of the adsorbent surface.[57]

3.3.2. Effect of adsorbent dosage. As illustrated in Fig. S1, the removal efficiency of CV is strongly influenced by the amount of adsorbent used, revealing a direct correlation between adsorbent dosage and adsorption performance. This trend arises from the increasing availability of active surface sites and the larger specific surface area at higher doses, which enhance the interaction between the dye molecules and the adsorbent.[58] Nevertheless, beyond a certain threshold, this effect stabilizes as adsorption sites begin to overlap or aggregate, leading to a slight decline in adsorption capacity.[59] The observed results indicate that the optimal adsorbent dose for efficient CV removal is 0.025 g, achieving removal efficiencies of

Table 3 Kinetics models parameters

	PFO					PSO		Intraparticle diffusion	
Model	C_0 (mg L^{-1})	q_{exp} (mg g^{-1})	q_{cal} (mg g^{-1})	k_1 (min^{-1})	R^2	q_{cal} (mg g^{-1})	k_2 (g mg^{-1} min^{-1})	R^2	k_{Int} (mg g^{-1} $min^{-1/2}$)	R^2
PPP/Sn–Fe	5	4.54	4.45	0.58	0.99	4.47	0.94	0.99	0.28	0.61
	10	9.82	9.13	2.19	0.90	10.2	0.02	0.99	0.65	0.68
	20	14.9	15.5	0.06	0.91	16.9	0.01	0.95	1.12	0.87
	50	50.3	45.1	9.19	0.70	53.3	0.01	0.97	3.26	0.65
	100	96.3	88.1	17.2	0.91	94.9	0.01	0.99	5.73	0.62
PPP/Sn–Zn	5	4.87	4.86	0.47	0.99	4.93	0.83	0.99	0.36	0.64
	10	9.60	9.37	0.16	0.99	9.99	0.02	0.99	0.62	0.65
	20	16.2	15.3	0.23	0.93	16.2	0.02	0.97	0.98	0.74
	50	50.6	48.2	9.90	0.94	51.0	0.01	0.99	2.72	0.51
	100	96.6	93.8	18.4	0.97	96.9	0.01	0.99	5.15	0.57

98.2% for PPP/Sn–Fe and 96.4% for PPP/Sn–Zn. These findings emphasize the importance of accurately optimizing the adsorbent dosage to ensure maximum removal efficiency in practical applications.

3.3.3. Effect of initial pH. The influence of pH on CV dye adsorption by PPP/Sn–Fe and PPP/Sn–Zn was evaluated over a pH range of 2–10, using an initial dye concentration of 10 mg L^{-1}, an adsorbent dose of 0.025 g, and a stirring speed of 250 rpm at room temperature (Fig. S1). The pH was adjusted with 1 M HCl and NaOH solutions. Both adsorbents exhibited consistently high removal efficiencies, ranging from 98.9% to 97.8% for PPP/Sn–Fe and 98.5% to 96.7% for PPP/Sn–Zn. These results confirm the comparable performance of both materials across a broad pH range, indicating that pH adjustment of water samples may not be required to ensure effective dye removal.

3.3.4. The influence of temperature. The influence of temperature on CV dye adsorption by PPP/Sn–Fe and PPP/Sn–Zn was investigated between 20 and 60 °C (Fig. S1). As temperature increased, the removal efficiency rose progressively, reaching 98.5% and 97.5% at 60 °C for PPP/Sn–Fe and PPP/Sn–Zn, respectively. This enhancement can be attributed to the reduction in solution viscosity and the consequent improvement in adsorbate diffusion and interaction with active sites. The observed trend confirms the endothermic nature of the adsorption process.[60]

3.4. Adsorption kinetics and isotherms

The adsorption kinetics of CV dye onto PPP/Sn–Fe and PPP/Sn–Zn were analyzed using pseudo-first-order, pseudo-second-order, and intraparticle diffusion models for concentrations ranging from 5 to 100 mg L^{-1}. Fig. S2(a–j) and S3(a–j) correspond to the PFO/PSO and intraparticle diffusion models, respectively. The corresponding kinetic parameters are summarized in Table 3. The higher determination coefficients (R^2) and the strong agreement between experimental and calculated adsorption capacities indicate that the PSO model provides a superior fit for both adsorbents, compared to the first-order and intraparticle diffusion models.[61] This suggests that the adsorption process is primarily governed by chemisorption, involving chemical interactions between CV molecules and the active sites on the adsorbent surfaces.[62]

The adsorption behavior of CV dye onto PPP/Sn–Fe and PPP/Sn–Zn was evaluated using the Langmuir, Freundlich and Tamkin isotherm models. The fitting plots of these isotherm models are shown in Fig. S4, while the calculated parameters for the Langmuir (q_{max}, K_L), Freundlich ($1/n$, K_F) and Temkin (K_T, b_T) models, along with their correlation coefficients R^2 values for CV dye adsorption, are summarized in Table 4. The experimental data showed good agreement with Langmuir and Freundlish isotherm models. The Langmuir model describes monolayer adsorption on a homogeneous surface, while the Freundlich model, with high correlation coefficients, indicates adsorption on heterogeneous surfaces.[63,64] In contrast, the Temkin model exhibited the lowest correlation coefficients, indicating that the assumption of a linear decrease in adsorption energy with increasing surface coverage is less applicable to the present adsorption system.[35] The maximum monolayer adsorption capacities (q_{max}) obtained from the Langmuir model were 675.47 mg g^{-1} for PPP/Sn–Fe and 357.18 mg g^{-1} for PPP/Sn–Zn, confirming the strong affinity of these materials for CV dye.

Table 4 Isotherms models parameters

		Parameters		
Isotherm model		q_{max} (mg g^{-1})	K_L (L mg^{-1})	R^2
Langmuir	PPP/Sn–Fe	675.47	0.03	0.98
	PPP/Sn–Zn	357.18	0.01	0.99
		Parameters		
Isotherm model		K_F (mg g^{-1})	$1/n$	R^2
Freundlich	PPP/Sn–Fe	23.2	0.86	0.99
	PPP/Sn–Zn	20.4	0.85	0.99
		Parameters		
Isotherm model		b_T (J mol^{-1})	K_T (L mg^{-1})	R^2
Temkin	PPP/Sn–Fe	23.4	5.97	0.88
	PPP/Sn–Zn	25.0	4.03	0.86

The excellent fit of experimental adsorption data to both Langmuir and Freundlich isotherm models, evidenced by correlation coefficients (R^2) approaching unity for each, indicates that the pomegranate peel biosorbent exhibits a hybrid adsorption mechanism involving both monolayer and multilayer processes. While the Langmuir model assumes homogeneous surface sites with uniform monolayer coverage and no adsorbate interaction, the Freundlich model accommodates heterogeneous surfaces permitting multilayer adsorption and site energy variation; the concurrent applicability of both suggests a surface with distinct homogeneous domains (favoring Langmuir behavior) alongside heterogeneous regions (aligning with Freundlich characteristics). This dual fitting is thus interpreted as initial monolayer adsorption saturating high-affinity sites, followed by multilayer formation at higher adsorbate concentrations, a phenomenon commonly observed

Table 5 Thermodynamic parameters at different temperatures

Biosorbents	T (°K)	$\Delta G°$ (kJ mol^{-1})	$\Delta H°$ (kJ mol^{-1})	$\Delta S°$ (J mol^{-1} K^{-1})
PPP/Sn–Fe	293	−5.46	35.3	139.0
	303	−6.53		
	313	−8.84		
	323	−9.38		
	333	−10.9		
PPP/Sn–Zn	293	−6.65	12.4	64.7
	303	−7.11		
	313	−7.61		
	323	−8.60		
	333	−9.12		

in complex biosorbents with diverse functional groups.[65] The Freundlich constant ($1/n$), reflecting adsorption favorability within the studied concentration range, was 0.86 for PPP/Sn–Fe and 0.85 for PPP/Sn–Zn, confirming their strong affinity for CV molecules. Moreover, the dimensionless separation factor (R_L) values of 0.74 and 0.65, respectively, further demonstrate that the adsorption process is favorable for both materials.

3.5. Adsorption thermodynamics

Thermodynamic parameters such as Gibbs free energy, enthalpy, and entropy ($\Delta G°$, $\Delta H°$, and $\Delta S°$) were evaluated to elucidate the nature of CV dye adsorption on PPP/Sn–Fe and PPP/Sn–Zn surfaces. The parameters were derived from the linear plot of $\ln K_D$ *versus* $1/T$ (Fig. S5), with $\Delta H°$ and $\Delta S°$ obtained from the slope and intercept, respectively (Tables S4 and 5).[66] Negative $\Delta G°$ values confirm the spontaneous nature of adsorption, while the positive $\Delta H°$ values (35.3 kJ mol^{-1} for PPP/Sn–Fe and 12.4 kJ mol^{-1} for PPP/Sn–Zn) indicate an endothermic process.[67,68] The relatively low enthalpy values (<40 kJ mol^{-1}) suggest that physical adsorption predominates. Moreover, the positive entropy changes (139.0 and 64.7 J mol^{-1} K^{-1}) reflect increased randomness at the solid–liquid interface,

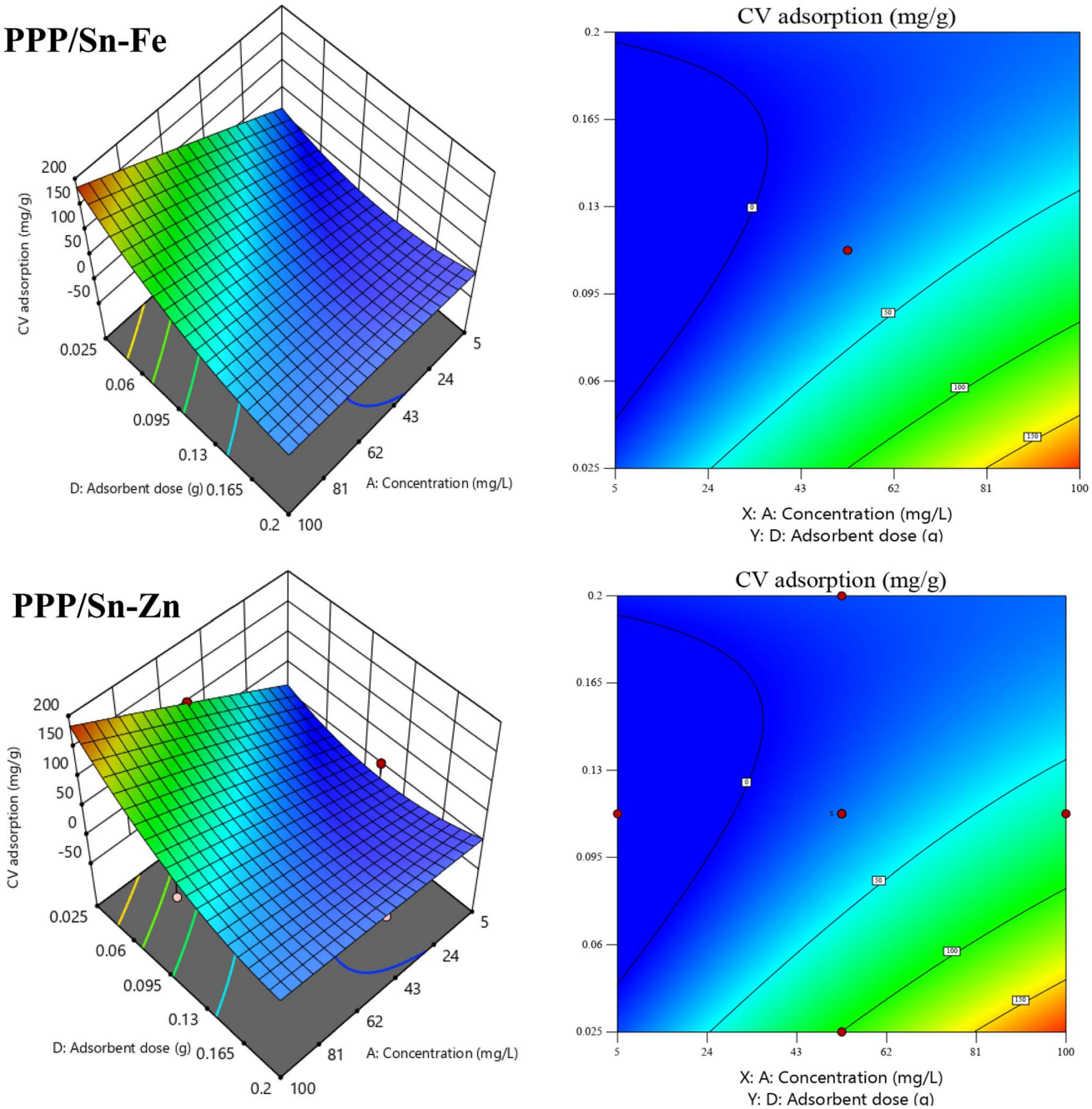

Fig. 6 The 3D response surface plots and contour plots for interactive effect of initial concentration and biosorbent dosage (CCD model).

likely due to the displacement of solvent molecules by CV dye during adsorption Table 5.

3.6. Design of experiments by CCD

The ANOVA results show that all main factors, such as initial dye concentration (A), pH (B), temperature (C), and biosorbent dose (D) significantly influence adsorption efficiency, which aligns with the known mechanisms of dye uptake involving electrostatic interactions, diffusion, and available active sites. Additionally, the significant two-level interaction between biosorbent dose and dye concentration (AD) indicates that the effect of concentration on adsorption is strongly dependent on the number of available active sites, a relationship consistent with adsorption saturation behavior. Because these interaction terms played an important role, the Reduced Quadratic Model was selected as the most appropriate representation of the system (Tables S8 and S10). The *p*-values (probability values) associated with the model terms in the ANOVA confirm the robustness and reliability of the models used to predict process responses.[69] Overall, this statistical analysis validates the influence of experimental parameters and their interactions in the biosorption process and justifies the use of CCD models for optimizing the experimental conditions of the biosorbents studied. The final regression models are expressed by the following equations eqn (6) and (7).

$$\text{CCD model (PPP/Sn–Fe)} = +22.18 + 45.59A - 41.90D - 37.55\text{AD} + 32.18D^2 \quad (6)$$

$$\text{CCD Model (PPP/Sn–Zn)} = +22.32 + 46.37A - 42.99D - 38.43\text{AD} + 33.18D^2 \quad (7)$$

The correlation coefficients (R^2 and adjusted R^2) for CCD model, summarized in Tables S5–S8, were close to unity, demonstrating an excellent agreement between experimental and predicted values. Specifically, R^2 values of 0.9777 and 0.9841 were obtained for PPP/Sn–Fe and PPP/Sn–Zn. The close proximity between R^2 and adjusted R^2 values further confirms the robustness and predictive reliability of the proposed models. Moreover, the high Fisher's F-statistics (262.95 and 370.63) and *p*-values below 0.05 validate the strong statistical significance of both models in describing the adsorption process.

Three-dimensional surface plots and two-dimensional contour maps (Fig. 6) were generated from the quadratic models given in eqn (6) and (7) to visualize the effects and interactions of the studied parameters.[70,71] These graphical representations reveal that the initial concentration and biosorbent dose are among the most significant variables affecting the responses. The CV adsorption increased with a decrease in biosorbent dose as shown in Fig. 6 (The transition from the blue zone to the red zone signifies the progression from minimum to maximum CV adsorption). When the surface area of adsorbents increases and more adsorption sites become available for a constant quantity of adsorption particles, it facilitates the overlap ping of adsorption sites, thereby leading to a reduction in adsorption capacity. The increase in the initial CV dye con centration from 5 to 100 mg L^{-1} resulted in an increase in the response. This in turn would increase the driving force for mass transfer and therefore the rate at which CV ions pass from the solution to the particle surface.

3.7. Multi-response optimization based on desirability criteria

The RSM optimization aimed to identify the optimal conditions for maximizing adsorption performance, with accuracy

Table 6 CV dye adsorption on regenerated PPP/Sn–Fe and PPP/Sn–Zn biosorbents

Number of cycle	1	2	3	4	5	6	7
Adsorption capacities (mg g^{-1})							
PPP/Sn–Fe	183.1	197.9	177.8	169.7	160.1	159.7	159.5
PPP/Sn–Zn	183.4	182.7	180.3	176.8	171.5	171.4	171.4

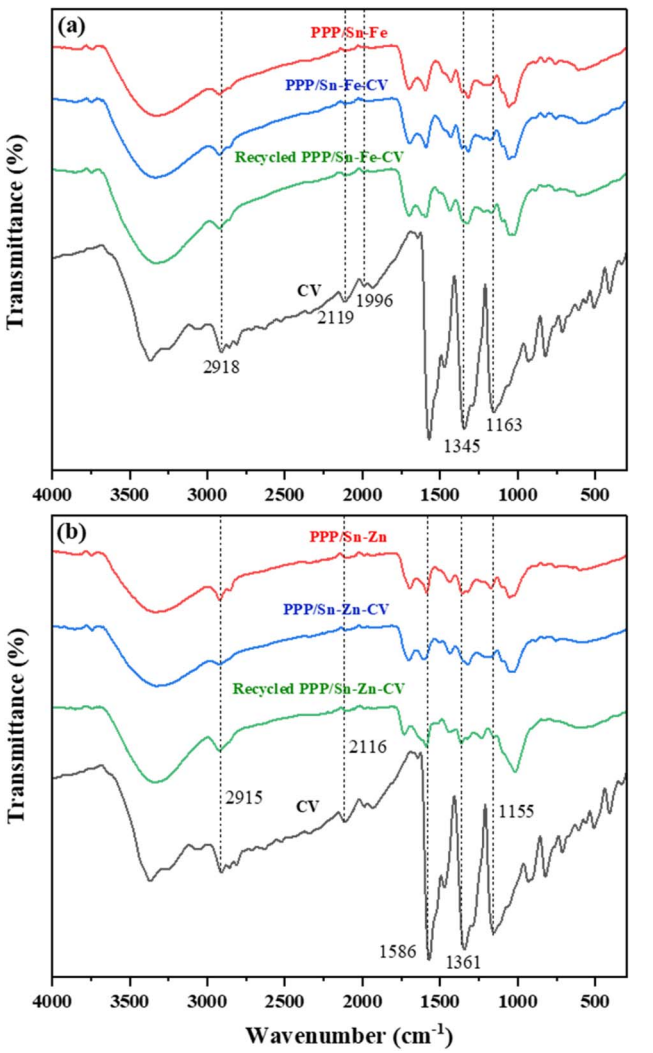

Fig. 7 FTIR spectra of (a) PPP/Sn–Fe, PPP/Sn–Fe-CV, recycled PPP/Sn–Fe-CV, CV and (b) PPP/Sn–Zn, PPP/Sn–Zn-CV, recycled PPP/Sn–Zn-CV and CV. Dotted lines highlight the FTIR bands from CV dye.

depending on the defined experimental boundaries rather than achieving a perfect desirability value of 1.0. The optimization plots for the CCD model (Fig. S6) revealed ideal parameters for CV dye adsorption at an initial concentration of 100 mg L^{-1}, pH 6, temperature of 40 °C, and an adsorbent dose of 0.025 g for both PPP/Sn–Fe and PPP/Sn–Zn. The CCD model provided slightly higher values of 189.12 and 187.05 mg g^{-1}, each with a desirability of 0.996. These findings demonstrate that CCD model confirming the robustness of the RSM-based optimization for efficient CV dye removal.

Based on this model, the optimal adsorption performance for CV dye removal was evaluated under the optimized parameters. The experimental and predicted capacities were 192.67 and 189.12 mg g^{-1} for PPP/Sn–Fe, and 192.62 and 187.62 mg g^{-1} for PPP/Sn–Zn, respectively. The close agreement between experimental and predicted values confirms the reliability in accurately describing the CV dye adsorption process.

3.8. Reusability of the various adsorbents

After the adsorption and optimization experiments, the regeneration process consisted of desorbing the CV dye from the saturated biosorbents, recovering them by filtration, washing repeatedly with distilled water, and finally drying at 80 °C to restore their adsorption capacity for reuse. The reusability of PPP/Sn–Fe and PPP/Sn–Zn was evaluated using 0.025 g of adsorbent in contact with 50 mL of crystal violet solution under the optimal adsorption conditions determined in this study (initial CV concentration of 100 mg L^{-1}, pH 6, and temperature 40 °C). Both materials exhibited excellent stability over successive adsorption–desorption cycles.[72] After seven cycles, the CV adsorption capacity showed only a moderate decline, decreasing from from 183.1 mg g^{-1} to 159.5 mg g^{-1} for PPP/Sn–Fe and from 183.4 mg g^{-1} to 171.4 mg g^{-1} for PPP/Sn–Zn. These findings confirm the strong regeneration potential and long-term applicability of the modified biosorbents for dye-

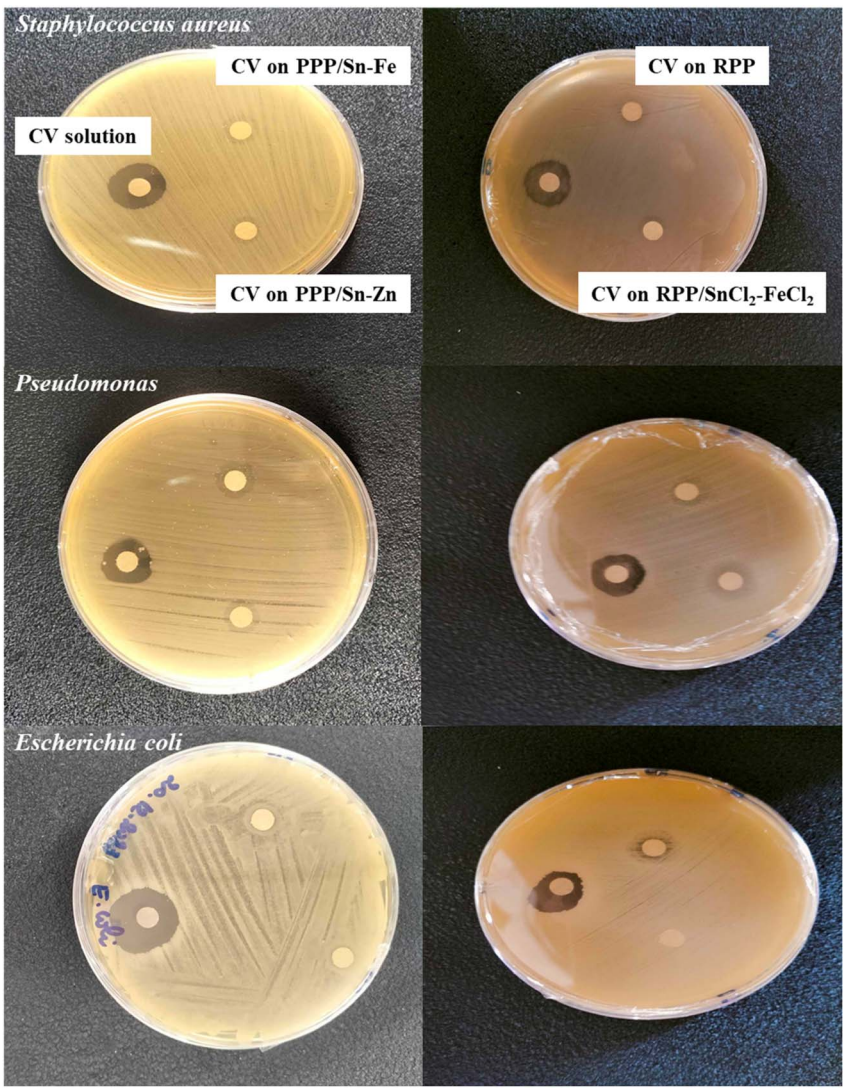

Fig. 8 The assay on microbial toxicity displays the impact of untreated and treated CV dye solution on three types of bacteria (m = 0.025 g, C = 100 mg L^{-1}, V = 50 mL).

contaminated wastewater treatment.[42] The corresponding adsorption capacities are presented in Table 6.

Furthermore, the successful regeneration of PPP/Sn–Fe and PPP/Sn–Zn was corroborated by FTIR analysis (Fig. 7). After adsorption, several characteristic vibrational bands associated with CV dye were observed in the spectra of both materials, confirming effective dye uptake. Overall, PPP/Sn–Fe and PPP/Sn–Zn can be regarded as highly competitive biosorbents that can be reused multiple times without significant deterioration of their adsorption performance.

3.9. Adsorption mechanisms of CV onto PPP/Sn–Fe and PPP/Sn–Zn

The adsorption of the cationic crystal violet dye onto both composite adsorbents PPP/Sn–Fe and PPP/Sn–Zn, is governed by a combination of key physicochemical interactions. Electrostatic attraction is considered the primary driving force, facilitated by the deprotonation of functional groups (such as carboxyl and hydroxyl groups) on the pomegranate peel -derived matrix, resulting in a negatively charged surface that strongly attracts the positively charged CV molecule. This interaction is highly sensitive to the solution pH and the point of zero charge (pH_{PZC}) of the materials. Furthermore, the aromatic nature of the CV molecule and the conjugated structures inherent to the biomass backbone promote significant π–π stacking interactions, which provide strong chemical stability to the adsorbed dye layer. Finally, Hydrogen bonding also contributes to the overall stability, forming between the surface's hydroxyl/carbonyl groups and the nitrogen atoms and polarized C–H bonds of the CV dye.[47,73] While these core mechanisms are shared, the specific metal ions (Fe^{3+} *versus* Zn^{2+}) incorporated in the composites are anticipated to influence the surface properties, porosity, and availability of Lewis acid sites, subtly modulating the overall adsorption capacity and efficiency, particularly in relation to complexation or specific binding with the dye molecule.

3.10. Microbial toxicity findings

Microbial toxicity tests revealed that the CV stock solution (100 mg L^{-1}) produced inhibition zones exceeding 20 mm, indicating strong toxicity toward *E. coli*, *Pseudomonas*, and *Staphylococcus aureus*. In contrast, the CV solutions treated with PPP/Sn–Fe and PPP/Sn–Zn exhibited negligible inhibition, as illustrated in Fig. 8. This demonstrates that adsorption effectively reduces CV toxicity compared with previously studied biosorbents, particularly natural materials such as unmodified pomegranate peel.[42] The absence of microbial inhibition further confirms that the treated effluents are environmentally safe and non-toxic.

Table 7 Comparison of different adsorbents based on CV dye sorption capacity (mg g^{-1})

Adsorbents	Modification	Experimental conditions	q_{max} (mg g^{-1})	Ref.
PPP/Sn–Fe	$SnCl_2$–$FeCl_3$	[CV] = 100 mg L^{-1} m = 0.025 g	675.47	Our work
PPP/Sn–Zn	$SnCl_2$–$ZnCl_2$	pH = 6 T = 40 °C	357.18	
Raw pomegranate peel (RPP)	—	[CV] = 100 mg L^{-1} m = 0.025 g	172.40	42
RPP/$SnCl_2$–$FeCl_2$	$SnCl_2$–$FeCl_2$	pH = 6 T = 40 °C	389.88	
Date pits powder/sodium alginate	NaOH	[CV] = 50 mg L^{-1} m = 0.02 g	169.88	74
Xanthated rice husks (XRH)	NaOH/CS_2	m = 0.025 g pH = 10	90.02	75
Coconut husk powder (CHP)	H_2SO_4	[CV] = 200 mg L^{-1} pH = 5 T = 45 °C	500.00	60
Magnetized bentonite clay particles (MBCP)	Fe_3O_4	T = 30 °C	588.23	76
Natural zeolite	—	pH = 6 T = 40 °C	177.75	77
Leaves of *Suaeda monoica* (LP)	$NiCuZnFe_2O_4$–biochar (300 °C)	[CV] = 200 mg L^{-1} m = 0.03 g pH = 8	325.50	68
Fe- benzene dicarboxylic acid MOF	—	[CV] = 5 mg L^{-1}	26.65	78
Metal–organic framework PCN-222(Fe)	HCl/DMF activation (120 °C)	[CV] = 200 mg L^{-1} $m \sim 0.003$ g pH = 7 T = 25 °C	812	79
TFPB-Pa-SO_3H COF TFPB-BDSA COF	Sulfonation (–SO_3H)	[CV] = 20 mg L^{-1} m = 0.005 g	1559 1288	80
TpStb-SO_3Na COF	Schiff-base condensation of Tp and Stb-SO_3H	[CV] = 30 mg L^{-1} T = 25 °C	1861	81

3.11. Comparative investigation on adsorption performance

A comparative assessment of the results demonstrates that the PPP/Sn–Fe and PPP/Sn–Zn adsorbents exhibit outstanding performance for CV dye removal from aqueous solutions. The adsorption capacities achieved in this work exceed those reported in most previous studies (Table 7), underscoring the remarkable efficiency of these materials. These findings emphasize the strong potential of pomegranate peel–based adsorbents as sustainable and effective candidates for the treatment of CV-contaminated wastewater.

4. Conclusion

In this study, biosorbents modified with $SnCl_2$–$FeCl_3$ and $SnCl_2$–$ZnCl_2$ were successfully evaluated for the removal of crystal violet (CV) from aqueous solutions. The investigation of key experimental parameters, including contact time, pH, temperature, initial dye concentration, and biosorbent dosage, provided a thorough understanding of the factors influencing adsorption efficiency. The application of Response Surface Methodology (RSM) with Central Composite Design (CCD) enabled the systematic optimization of these parameters, ensuring maximum dye removal. The adsorption behavior was accurately described using appropriate isotherm and kinetic models, confirming the suitability of the developed biosorbents for efficient dye uptake. Importantly, the reusability tests demonstrated that the materials maintained high adsorption performance over multiple cycles, highlighting their practical potential. Overall, the study not only elucidates the activation and adsorption mechanisms of $SnCl_2$-based biosorbents but also provides optimized formulations that are promising for scalable, sustainable treatment of dye-contaminated wastewater, aligning with environmental and industrial application goals.

Conflicts of interest

There are no conflicts to declare.

Data availability

The data supporting the findings of this study are available within the article and its supplementary information (SI). Supplementary information: additional experimental data, spectra, and detailed tables supporting the results presented in the main manuscript. See DOI: https://doi.org/10.1039/d5ra09290f.

References

1 T. Akter, A. T. Prottity, M. Shaha, M. Al Mamun, and A. Hashem, The Impact of Textile Dyes on the Environment, *Nanohybrid Materials for Treatment of Textiles Dyes, Nanohybrid Materials for Treatment of Textiles Dyes*, A. Ahmad, M. Jawaid, M. N. Mohamad Ibrahim, A. A. Yaqoob and M. B. Alshammari, 2023, 401–431, DOI: 10.1007/978-981-99-3901-5_17.

2 N. Bouzenad, N. Ammouchi, N. Chaib, Y. Belhocine, A. Belhaoues, N. Hamrouche, S. E. I. Boudagha, A. Abdennouri and W. Zahnit, Development of Bioplastic Films from Sargassum muticum Alginate: Properties and Applications in Food Packaging, *Iran. J. Chem. Chem. Eng.*, 2024, **43**(10), 3794–3811, DOI: 10.30492/ijcce.2024.2023449.6460.

3 N. Bouzenad, N. Ammouchi, A. Abdennouri, A. Bouzana, H. A. Rudayni, F. Boufahja and H. Bendif, Comprehensive review of alginate: Sources, synthesis, and application in the food packaging sector, *Ital. J. Food Sci.*, 2025, **37**(4), 1–15, DOI: 10.15586/ijfs.v37i4.3033.

4 E. O. Alegbe and T. O. Uthman, A review of history, properties, classification, applications and challenges of natural and synthetic dyes, *Heliyon*, 2024, **10**(13), e33646, DOI: 10.1016/j.heliyon.2024.e33646.

5 A. S. Alawam, S. M. Mahgoub, A. A. Allam, A. M. Radalla, M. H. Shemy and R. Mahmoud, Sustainable zeolite/activated carbon nanocomposite for dual-dye adsorption, kinetic and thermodynamic studies, and urea electro-oxidation applications, *RSC Adv.*, 2025, **15**(51), 43983–44006, DOI: 10.1039/D5RA06559C.

6 S. Dutta, B. Gupta, S. K. Srivastava and A. K. Gupta, Recent advances on the removal of dyes from wastewater using various adsorbents: a critical review, *Mater. Adv.*, 2021, **2**(14), 4497–4531, DOI: 10.1039/D1MA00354B.

7 L. T. K. Thoa, T. T. P. Thao, M.-L. Nguyen-Thi, N. D. Chung, C. W. Ooi, S.-M. Park, T. T. Lan, H. T. Quang, K. S. Khoo, P. L. Show and N. D. Huy, Microbial biodegradation of recalcitrant synthetic dyes from textile-enriched wastewater by Fusarium oxysporum, *Chemosphere*, 2023, **325**, 138392, DOI: 10.1016/j.chemosphere.2023.138392.

8 O. T. Mahlangu, G. Mamba and B. B. Mamba, A facile synthesis approach for GO-ZnO/PES ultrafiltration mixed matrix photocatalytic membranes for dye removal in water: Leveraging the synergy between photocatalysis and membrane filtration, *J. Environ. Chem. Eng.*, 2023, **11**(3), 110065, DOI: 10.1016/j.jece.2023.110065.

9 F. N. Türk, H. Çiftçi and H. Arslanoğlu, Removal of Basic Yellow 51 Dye by Using Ion Exchange Resin Obtained by Modification of Byproduct Sugar Beet Pulp, *Sugar Technol.*, 2023, **25**(3), 569–579, DOI: 10.1007/s12355-022-01207-2.

10 T. Xu L Fu, H. Lu, M. Zhang, W. Wang, B. Hu, Y. Zhou and G. Yu, Electrochemical oxidation degradation of Rhodamine B dye on boron-doped diamond electrode: Input mode of power attenuation, *J. Clean. Prod.*, 2023, **401**, 136794, DOI: 10.1016/j.jclepro.2023.136794.

11 D. S. B. Ali, F. Krid, A. Sarra Saadi, M. Nacef, H. Tabet and M. Lyamine Chelaghmia, Simultaneous electrochemical detection of Cd 2+ and Pb 2+ using a green silver nanoparticles/polyaniline-modified carbon paste electrode, *RSC Adv.*, 2025, **15**(36), 29654–29665, DOI: 10.1039/D5RA03135D.

12 K. S. A. Sahoo, J. Kumar, A. Kumari, K. K. Pant, A. Bhatnagar and T. Bhaskar, Effective utilization of discarded reverse

osmosis post-carbon for adsorption of dyes from wastewater, *Environ. Res.*, 2023, **231**, 116165, DOI: 10.1016/j.envres.2023.116165.

13 A. Mancuso N Blangetti, O. Sacco, F. S. Freyria, B. Bonelli, S. Esposito, D. Sannino and V. Vaiano, Photocatalytic Degradation of Crystal Violet Dye under Visible Light by Fe-Doped TiO2 Prepared by Reverse-Micelle Sol–Gel Method, *Nanomaterials*, 2023, **13**(2), 270, DOI: 10.3390/nano13020270.

14 M. Khatri, R. A. Al-Juboori, M. Mehdi, N. K. Khanzada, and N. Hilal, Adsorption Techniques for Dye Removal/Recovery from Industrial Wastewater, in *Water Treatment*, CRC Press., 2025, 82–108, doi: DOI: 10.1201/9781003471998_6.

15 D. C. L. Kon, S.-F. Lim, D. S. N. Chua and B. H. Lim, Synthesis of coconut husk-derived partially oxidised graphene oxide for methylene blue dye removal, *J. Indian Chem. Soc.*, 2025, **102**(9), 101880, DOI: 10.1016/j.jics.2025.101880.

16 J. B. Haider, M. I. Haque, M. Hoque, M. M. Hossen, M. Mottakin, M. A. Khaleque, M. A. H. Johir, J. L. Zhou, M. B. Ahmed and M. Zargar, Efficient extraction of silica from openly burned rice husk ash as adsorbent for dye removal, *J. Clean. Prod.*, 2022, **380**, 135121, DOI: 10.1016/j.jclepro.2022.135121.

17 U. Maheshwari, R. V. Thakur, D. Deshpande and S. Ghodke, Efficiency evaluation of orange and banana peels for dye removal from synthetic industrial effluent, *Mater. Today: Proc.*, 2023, **76**, 170–176, DOI: 10.1016/j.matpr.2022.11.023.

18 M. Hasan, M. T. Al Biruni, S. Azad and T. Ahmed, Adsorptive removal of dye from textile wastewater employing Moringa oleifera leaves biochar as a natural biosorbent, *Biomass Convers. Biorefinery*, 2024, **14**(10), 11075–11091, DOI: 10.1007/s13399-022-03196-4.

19 S. Wong, S. Wong, N. A. Ghafar, N. Ngadi, F. A. Razmi, I. M. Inuwa, R. Mat and N. A. S. Amin, Effective removal of anionic textile dyes using adsorbent synthesized from coffee waste, *Sci. Rep.*, 2020, **10**(1), 2928–2020, DOI: 10.1038/s41598-020-60021-6.

20 R. Atef, N. M. Aboeleneen and N. M. AbdelMonem, Preparation and characterization of low-cost nano-particle material using pomegranate peels for brilliant green removal, *Int. J. Phytoremediation*, 2023, **25**(1), 36–46, DOI: 10.1080/15226514.2022.2056133.

21 A. K. Tolkou, E. K. Tsoutsa, I. A. Katsoyiannis and G. Z. Kyzas, Simultaneous removal of anionic and cationic dyes on quaternary mixtures by adsorption onto banana, orange and pomegranate peels, *Colloids Surf., A*, 2024, **685**, 133176, DOI: 10.1016/j.colsurfa.2024.133176.

22 S. Ben-Ali, Application of Raw and Modified Pomegranate Peel for Wastewater Treatment: A Literature Overview and Analysis, *Int. J. Chem. Eng.*, 2021, **2021**, e8840907, DOI: 10.1155/2021/8840907.

23 B. R. Poudel, R. L. Aryal, S. K. Gautam, K. N. Ghimire, H. Paudyal and M. R. Pokhrel, Effective Remediation of Arsenate from Contaminated Water by Zirconium Modified Pomegranate Peel as an Anion Exchanger, *J. Environ. Chem. Eng.*, 2021, **9**(6), 106552, DOI: 10.1016/j.jece.2021.106552.

24 J. Bedia, M. Peñas-Garzón, A. Gómez-Avilés, J. J. Rodriguez and C. Belver, Review on Activated Carbons by Chemical Activation with FeCl3, *J. Carbon Res.*, 2020, **6**(2), 21, DOI: 10.3390/c6020021.

25 M. Zhong, X. Liu, J. Ma and L. Shang, Bamboo-Activated Carbon Synthesized by One-Pot Pyrolysis and $FeCl_2$ Activation for the Removal of Cr(VI) in Aqueous Solutions, *Water*, 2023, **15**(10), 1891, DOI: 10.3390/w15101891.

26 H. Zhao, H. Zhong, Y. Jiang, H. Li, P. Tang, D. Li and Y. Feng, Porous $ZnCl_2$-Activated Carbon from Shaddock Peel: Methylene Blue Adsorption Behavior, *Materials*, 2022, **15**(3), 895, DOI: 10.3390/ma15030895.

27 S. Karishma, V. C. Deivayanai, P. Thamarai, A. Saravanan and P. R. Yaashikaa, Adsorption Dynamics of Eriochrome Black Dye Removal Using Raw and Ultrasonicated Pithecellobium Seed Biomass: ANN Modeling and Mechanisms, *Sustain. Chem. Environ.*, 2024, **7**, 100143, DOI: 10.1016/j.scenv.2024.100143.

28 M. Reji and R. Kumar, Response surface methodology (RSM): An overview to analyze multivariate data, *Indian J. Microbiol. Res.*, 2022, **9**, 241–248, DOI: 10.18231/j.ijmr.2022.042.

29 M. A. Ahmad, M. A. Eusoff, P. O. Oladoye, K. A. Adegoke and O. S. Bello, Optimization and batch studies on adsorption of Methylene blue dye using pomegranate fruit peel based adsorbent, *Chem. Data Collect.*, 2021, **32**, 100676, DOI: 10.1016/j.cdc.2021.100676.

30 S. Narukulla, S. Narukulla, S. Bogadi, V. Tallapaneni, B. K. R. Sanapalli, S. Sanju, A. A. Khan, A. Malik, H. R. Barai, T. K. Mondal, V. V. S. R. Karri, A. Alexiou, S. K. S. S. Pindiprolu, G. Kuppusamy, V. Subramaniyan, M. R. Islam and M. Papadakis, Comparative study between the Full Factorial, Box–Behnken, and Central Composite Designs in the optimization of metronidazole immediate release tablet, *Microchem. J.*, 2024, **207**, 111875, DOI: 10.1016/j.microc.2024.111875.

31 M. T. M. Hussien Hamad, Optimization study of the adsorption of malachite green removal by MgO nano-composite, nano-bentonite and fungal immobilization on active carbon using response surface methodology and kinetic study, *Environ. Sci. Eur.*, 2023, **35**(1), 26, DOI: 10.1186/s12302-023-00728-1.

32 Z. H. Mussa, L. R. Al-Ameer, F. F. Al-Qaim, I. F. Deyab, H. Kamyab and S. Chelliapan, A comprehensive review on adsorption of methylene blue dye using leaf waste as a bio-sorbent: isotherm adsorption, kinetics, and thermodynamics studies, *Environ. Monit. Assess.*, 2023, **195**(8), 940, DOI: 10.1007/s10661-023-11432-1.

33 Y. Song, R. Peng, S. Chen and Y. Xiong, Adsorption of crystal violet onto epichlorohydrin modified corncob, *Cell.*, 2019, **1**, 5, DOI: 10.5004/dwt.2019.24067.

34 A. C. R. W. Moreira, B. B. Ferri, D. F. Santos, M. H. N. O. Scaliante, E. C. N. F. Duarte and R. Bergamasco, Ibuprofen removal by modified natural zeolite: characterization, modeling, and adsorption mechanisms, *J. Chem. Technol. Biotechnol.*, 2024, **99**(11), 2407–2419, DOI: 10.1002/jctb.7729.

35 A. S. Saadi, D. Slimane Ben Ali and S. Bousba, Utilization of a biosorbent derived from plant residues for the treatment of water contaminated with rhodamine B: preparation and characterization, *RSC Adv.*, 2025, **15**(50), 43038–43052, DOI: 10.1039/D5RA07130E.

36 E. Khanniri, M. Yousefi, A. M. Mortazavian, N. Khorshidian, S. Sohrabvandi, M. Arab and M. R. Koushki, Effective removal of lead (II) using chitosan and microbial adsorbents: Response surface methodology (RSM), *Int. J. Biol. Macromol.*, 2021, **178**, 53–62, DOI: 10.1016/j.ijbiomac.2021.02.065.

37 S. Sun, Y. Zhu, Z. Gu, H. Chu, C. Hu, L. Gao and X. Zhao, Adsorption of crystal violet on activated bamboo fiber powder from water: preparation, characterization, kinetics and isotherms, *RSC Adv.*, 2023, **13**(9), 6108–6123, DOI: 10.1039/D2RA08323J.

38 M. Mansouri, M. Shayanmehr and A. Ghaemi, Exploring the adsorption desulfurization efficiency using RSM and ANN methodologies, *Sci. Rep.*, 2025, **15**(1), 20869, DOI: 10.1038/s41598-025-05688-5.

39 S. Masoomeh Rahimi, A. Hossein Panahi, N. Sadat Mazari Moghaddam, E. Allahyari and N. Nasseh, Breaking Down of Low-Biodegradation Acid Red 206 Dye Using Bentonite/Fe_3O_4/ZnO Magnetic Nanocomposite as a Novel Photo-Catalyst in Presence of UV Light, *Chem. Phys. Lett.*, 2022, **794**, 139480, DOI: 10.1016/j.cplett.2022.139480.

40 B. Kakavandi, A. Takdastan, N. Jaafarzadeh, M. Azizi, A. Mirzaei and A. Azari, Application of Fe_3O_4@C Catalyzing Heterogeneous UV-Fenton System for Tetracycline Removal with a Focus on Optimization by a Response Surface Method, *J. Photochem. Photobiol. Chem.*, 2016, **314**, 178–188, DOI: 10.1016/j.jphotochem.2015.08.008.

41 Y. Rashtbari, S. Hazrati, A. Azari, S. Afshin, M. Fazlzadeh and M. Vosoughi, A Novel, Eco-Friendly and Green Synthesis of PPAC-ZnO and PPAC-nZVI Nanocomposite Using Pomegranate Peel: Cephalexin Adsorption Experiments, Mechanisms, Isotherms and Kinetics, *Adv. Powder Technol.*, 2020, **31**(4), 1612–1623, DOI: 10.1016/j.apt.2019.12.012.

42 N. Hamrouche, C. Djilani, P. Magri, Y. Belhocine, F. Djazi, M. Kezzar and N. Bouzenad, A novel biosorbent from raw pomegranate peel modified with SnCl2/FeCl2 for the adsorption of crystal violet cationic dye: response surface methodology process optimization, thermodynamic, kinetic, isotherm, and recyclability studies, *Biomass Convers. Biorefinery*, 2024, 15, DOI: 10.1007/s13399-024-05737-5.

43 M. Namvar-Mahboub, F. Ahsani and S. Ansari, Preparation and Characterization of Nanosized Pomegranate Peel-Based Activated Carbon for Application in Pyridine Removal from Aqueous Solution, *Theor. Found. Chem. Eng.*, 2020, **54**(5), 940–948, DOI: 10.1134/S0040579520050371.

44 D. Surendhiran, C. Li, H. Cui and L. Lin, Fabrication of High Stability Active Nanofibers Encapsulated with Pomegranate Peel Extract Using Chitosan/PEO for Meat Preservation, *Food Packag. Shelf Life*, 2020, **23**, 100439, DOI: 10.1016/j.fpsl.2019.100439.

45 M. Akram, X. Xu, B. Gao, S. Wang, R. Khan, Q. Yue, P. Duan, H. Dan and J. Pan, Highly efficient removal of phosphate from aqueous media by pomegranate peel co-doping with ferric chloride and lanthanum hydroxide nanoparticles, *J. Clean. Prod.*, 2021, **292**, 125311, DOI: 10.1016/j.jclepro.2020.125311.

46 N. Rouahna, D. Ben Salem, I. Bouchareb, A. Nouioua, A. Ouakouak, A. Fadel, N. Hamdi and R. Boopathy, Reduction of Crystal Violet Dye from Water by Pomegranate Peel–Derived Efficient Biochar: Influencing Factors and Adsorption Behaviour, *Water. Air. Soil Pollut.*, 2023, **234**(5), 324, DOI: 10.1007/s11270-023-06338-0.

47 A. Suhaimi, A. S. Abdulhameed, A. H. Jawad, T. A. Yousef, O. K. Al Duaij, Z. A. AlOthman and L. D. Wilson, Production of large surface area activated carbon from a mixture of carrot juice pulp and pomegranate peel using microwave radiation-assisted ZnCl2 activation: An optimized removal process and tailored adsorption mechanism of crystal violet dye, *Diam. Relat. Mater.*, 2022, **130**, 109456, DOI: 10.1016/j.diamond.2022.109456.

48 R. Rai, R. L. Aryal, H. Paudyal, S. K. Gautam, K. N. Ghimire, M. R. Pokhrel and B. R. Poudel, Acid-treated pomegranate peel; An efficient biosorbent for the excision of hexavalent chromium from wastewater, *Heliyon*, 2023, **9**(5), e15698, DOI: 10.1016/j.heliyon.2023.e15698.

49 A. Hariharan, V. Harini, S. Sandhya and S. Rangabhashiyam, Waste Musa acuminata residue as a potential biosorbent for the removal of hexavalent chromium from synthetic wastewater, *Biomass Convers. Biorefinery*, 2023, **13**(2), 1297–1310, DOI: 10.1007/s13399-020-01173-3.

50 M. A. Suleiman, M. A. A. Zaini and N. D. Mu'azu, Pomegranate peel adsorbents for water pollutants removal: preparation, characterization and applications, *Int. J. Phytoremediation*, 2025, **27**(8), 1119–1139, DOI: 10.1080/15226514.2025.2484292.

51 S. Dubey, R. Kumar and M. KumarMondal, Pyrolysis kinetics and thermodynamics of pomegranate peel usingTG/DTG analysis, *Biomass Convers. Biorefinery*, 2024, **14**(11), 12411–12425, DOI: 10.1007/s13399-022-03288-1.

52 S. Brunauer, P. H. Emmett and E. Teller, Adsorption of Gases in Multimolecular Layers, *J. Am. Chem. Soc.*, 1938, **60**(2), 309–319, DOI: 10.1021/ja01269a023.

53 S. Brunauer, L. S. Deming, W. E. Deming and E. Teller, On a theory of the van der Waals adsorption of gases, *J. Am. Chem. Soc.*, 1940, **62**(7), 1723–1732, DOI: 10.1021/ja01864a025.

54 R. C. Patil, U. P. Patil, A. A. Jagdale, S. K. Shinde and S. S. Patil, Ash of pomegranate peels (APP): A bio-waste heterogeneous catalyst for sustainable synthesis of α,α′-bis(substituted benzylidine)cycloalkanones and 2-arylidene-1-tetralones, *Res. Chem. Intermed.*, 2020, **46**(7), 3527–3543, DOI: 10.1007/s11164-020-04160-5.

55 B. M. Thamer, F. A. Al-Aizari and H. S. Abdo, Enhanced adsorption of textile dyes by a novel sulfonated activated carbon derived from pomegranate peel waste: isotherm, kinetic and thermodynamic study, *Molecules*, 2023, **28**(23), 7712, DOI: 10.3390/molecules28237712.

56 A. Hashem, C. O. Aniagor, M. Fikry, G. M. Taha and S. M. Badawy, Characterization and adsorption of raw pomegranate peel powder for lead (II) ions removal, *J. Mater. Cycles Waste Manag.*, 2023, **25**(4), 2087–2100, DOI: 10.1007/s10163-023-01655-2.

57 M. Abbas, Z. Harrache and M. Trari, Mass-transfer processes in the adsorption of crystal violet by activated carbon derived from pomegranate peels: Kinetics and thermodynamic studies, *J. Eng. Fibers Fabr.*, 2020, **15**, 155892502091984, DOI: 10.1177/1558925020919847.

58 M. T. Yagub, T. K. Sen, S. Afroze and H. M. Ang, Dye and its removal from aqueous solution by adsorption: A review, *Adv. Colloid Interface Sci.*, 2014, **209**, 172–184, DOI: 10.1016/j.cis.2014.04.002.

59 G. M Khairy, A. M. Hesham, H. E. S. Jahin, S. A. El-Korashy and Y. Mahmoud Awad, Green synthesis of a novel eco-friendly hydrochar from Pomegranate peels loaded with iron nanoparticles for the removal of copper ions and methylene blue from aqueous solutions, *J. Mol. Liq.*, 2022, **368**, 120722, DOI: 10.1016/j.molliq.2022.120722.

60 S. Sultana, K. Islam, M. A. Hasan, H. M. J. Khan, M. A. R. Khan, A. Deb, M. A. Raihan and M. W. Rahman, Adsorption of crystal violet dye by coconut husk powder: Isotherm, kinetics and thermodynamics perspectives, *Environ. Nanotechnol. Monit. Manag.*, 2022, **17**, 100651, DOI: 10.1016/j.enmm.2022.100651.

61 A. Essekri, M. Laabd and A. Albourine, Efficient adsorption of crystal violet dye using functionalized Argan shell: Experiments and statistical optimization modeling, *Colloids Surf., A*, 2024, **687**, 133401, DOI: 10.1016/j.colsurfa.2024.133401.

62 E. H. Chafyq, K. Legrouri, M. Aghrouch, M. Oumam, S. Mansouri, E. Khouya and H. Hannache, Adsorption of the crystal violet dye on an adsorbent material prepared from Moroccan oil shales, *J. Iran. Chem. Soc.*, 2023, **20**(2), 351–359, DOI: 10.1007/s13738-022-02665-x.

63 R. Mecheri, A. Zobeidi, S. Atia, S. N. Nacer, A. A. M. Salih, M. Benaissa, D. Ghernaout, S. Al Arni, S. Ghareba and N. Elboughdiri, Modeling and Optimizing the Crystal Violet Dye Adsorption on Kaolinite Mixed with Cellulose Waste Red Bean Peels: Insights into the Kinetic, Isothermal, Thermodynamic, and Mechanistic Study, *Materials*, 2023, **16**(11), 4082, DOI: 10.3390/ma16114082.

64 M. A. Usman, R. A. Aftab, S. Zaidi, S. M. Adnan and R. A. K. Rao, Adsorption of aniline blue dye on activated pomegranate peel: equilibrium, kinetics, thermodynamics and support vector regression modelling, *Int. J. Environ. Sci. Technol.*, 2022, **19**(9), 8351–8368, DOI: 10.1007/s13762-021-03571-0.

65 A. Syafiuddin, S. Salmiati, J. Jonbi and M. A. Fulazzaky, Application of the kinetic and isotherm models for better understanding of the behaviors of silver nanoparticles adsorption onto different adsorbents, *J. Environ. Manage.*, 2018, **218**, 59–70, DOI: 10.1016/j.jenvman.2018.03.066.

66 F. M. C. Djilani, N. Bougdah, N. Messikh, E. Boussaha, A. Moumen, C. Bouchalta and M. S. Medjram, Adsorption of methylene blue onto activated carbon prepared under N2/microwave radiation supported cobalt: kinetics, isotherms, and thermodynamics studies, *Desalination Water Treat.*, 2023, **284**(288–300), 288–300, DOI: 10.5004/dwt.2023.29289.

67 M. Sadoq, H. Atlas, S. Imame, A. Kali, A. Amar, I. Loulidi, M. Jabri, B.-E. Sadoq, M. Ouchabi, P. S. Abdullah and F. Boukhlifi, Elimination of crystal violet from aqueous solution by adsorption on naturel polysaccharide: Kinetic, isotherm, thermodynamic studies and mechanism analysis, *Arab. J. Chem.*, 2024, **17**(1), 105453, DOI: 10.1016/j.arabjc.2023.105453.

68 D. Mehta, P. N. Dave and V. V. Kumar, Toxic crystal violet dye removal by novel, eco-friendly seablite biochar–ferrite composite: adsorption isotherm, kinetics, and artificial neural network, *RSC Adv.*, 2025, **15**(40), 33189–33208, DOI: 10.1039/D5RA04604A.

69 N. A. A. C. Hassan, A. Hapiz, A. H. Jawad, Z. A. ALOthman and L. D. Wilson, Desirability function and Box-Behnken design optimization for crystal violet dye adsorption by palm date stone activated carbon, *Biomass Convers. Biorefinery*, 2025, **15**(5), 7913–7925, DOI: 10.1007/s13399-024-05710-2.

70 N. A. Jani, L. Haddad, A. S. Abdulhameed, A. H. Jawad, Z. A. ALOthman and Z. M. Yaseen, Modeling and optimization of the adsorptive removal of crystal violet dye by durian (Durio zibethinus) seeds powder: insight into kinetic, isotherm, thermodynamic, and adsorption mechanism, *Biomass Convers. Biorefinery*, 2024, **14**(11), 12441–12454, DOI: 10.1007/s13399-022-03319-x.

71 T. T. T. Nguyen, D. Q. Hoang, D. T. C. Nguyen and T. V. Tran, Adsorptive Optimization of Crystal Violet Dye Using Central Composite Rotatable Design and Response Surface Methodology: Statistical Analysis, Kinetic and Isotherm Studies, *Arab. J. Sci. Eng.*, 2023, **48**(7), 8835–8848, DOI: 10.1007/s13369-022-07391-3.

72 A. Abbaz, S. Arris, G. Viscusi, A. Ayat, H. Aissaoui and Y. Boumezough, Adsorption of safranin O dye by alginate/pomegranate peels beads: Kinetic, isotherm and thermodynamic studies, *Gels*, 2023, **9**(11), 916, DOI: 10.3390/gels9110916.

73 Z. H. Mussa, A. F. Imran, L. R. Al-Ameer, H. F. S. Al-Saedi, I. F. Deyab, F. F. A-Qaim and H. Kamyab, Utilizing Pomegranate Peel Biochar for Effective Malachite Green Adsorption, *Results Surf. Interfaces*, 2025, 100618, DOI: 10.1016/j.rsu.2025.100618.

74 A. Mokhtar, S. Abdelkrim, M. Hachemaoui, B. Boukoussa, W. Chaibi, A. Sardi, A. Djelad, M. Sassi, I. Issam, J. Iqbal, S. P. Patole and M. Abboud, Removal of crystal violet dye using a three-dimensional network of date pits powder/sodium alginate hydrogel beads: Experimental optimization and DFT calculation, *Int. J. Biol. Macromol.*, 2023, **251**, 126270, DOI: 10.1016/j.ijbiomac.2023.126270.

75 P. L. Homagai, R. Poudel, S. Poudel and A. Bhattarai, Adsorption and removal of crystal violet dye from aqueous solution by modified rice husk, *Heliyon*, 2022, **8**(4), DOI: 10.1016/j.heliyon.2022.e09261.

76 M. Ahmed and A. Nasar, Magnetized Bentonite Clay Particles: An Eco-Friendly and Economical Adsorbent for Efficient Remediation of Crystal Violet Dye-Polluted Water, *Arab. J. Sci. Eng.*, 2024, **49**(1), 801–813, DOI: 10.1007/s13369-023-08518-w.

77 M. Sarabadan, H. Bashiri and S. M. Mousavi, Removal of Crystal Violet Dye by an Efficient and Low Cost Adsorbent: Modeling, Kinetic, Equilibrium and Thermodynamic Studies, *Korean J. Chem. Eng.*, 2019, **36**(10), 1575–1586, DOI: 10.1007/s11814-019-0356-1.

78 S. Soni, P. K. Bajpai, D. Bharti, J. Mittal and C. Arora, Removal of Crystal Violet from Aqueous Solution Using Iron Based Metal Organic Framework, *Desalination Water Treat.*, 2020, **205**, 386–399, DOI: 10.5004/dwt.2020.26387.

79 M. Sarker, S. Shin, J. H. Jeong and S. H. Jhung, Mesoporous Metal-Organic Framework PCN-222(Fe): Promising Adsorbent for Removal of Big Anionic and Cationic Dyes from Water, *Chem. Eng. J.*, 2019, **371**, 252–259, DOI: 10.1016/j.cej.2019.04.039.

80 W. Zheng, A. Li, X. Wang, Z. Li, B. Zhao, L. Wang, W. Kan, L. Sun and X. Qi, Construction of Hydrophilic Covalent Organic Frameworks and Their Fast and Efficient Adsorption of Cationic Dyes from Aqueous Solution, *New J. Chem.*, 2022, **46**(46), 22185–22194, DOI: 10.1039/D2NJ04336J.

81 R. Li, X. Tang, J. Wu, K. Zhang, Q. Zhang, J. Wang, J. Zheng, S. Zheng, J. Fan, W. Zhang, X. Li and S. Cai, A Sulfonate-Functionalized Covalent Organic Framework for Record-High Adsorption and Effective Separation of Organic Dyes, *Chem. Eng. J.*, 2023, **464**, 142706, DOI: 10.1016/j.cej.2023.142706.